

## Synthesis and Characterization of $\text{Nb}_2\text{O}_5:\text{La}^{3+},\text{Eu}^{3+}$ Phosphors Obtained by the Non-Hydrolytic Sol-Gel Process

Carlos R. Matias,<sup>a</sup> Eduardo J. Nassar,<sup>a</sup> Marc Verelst<sup>b</sup> and Lucas A. Rocha<sup>\*,a</sup>

<sup>a</sup>Departamento de Química, Universidade de Franca (UNIFRAN),  
CP 82, 14404-600 Franca-SP, Brazil

<sup>b</sup>Centre d'Elaboration de Matériaux et d'Etudes Structurales (CNRS), BP 4347,  
31055 Toulouse CEDEX 4, France

The phosphor-converted light-emitting diode technique is an important solid-state illumination strategy. Sulfide-based materials are the most often employed red phosphors, but they are chemically unstable and present lower efficiency in comparison to the blue and green phosphors. Therefore, it is important to find a new red phosphor source that can emit intense red light while absorbing light in the near ultraviolet (UV) spectral region. This paper describes the photoluminescence properties of  $\text{Nb}_2\text{O}_5:\text{La}^{3+},\text{Eu}^{3+}$  obtained by the non-hydrolytic sol-gel process. The X-ray results indicated that the thermal treatment allowed to obtain the different crystalline structures such as, the orthorhombic and monoclinic phases for the  $\text{Nb}_2\text{O}_5$  and the orthorhombic phase for the  $\text{La}_2\text{Nb}_{10}\text{O}_{28}$ . This polymorphism was also confirmed by the Raman spectroscopy. The luminescence spectra revealed the existence of the  $\text{Eu}^{3+}$  ions in both crystalline phases for the samples annealed at higher temperature, depending of the excitation wavelength. The emission spectrum showed that increasing the annealing temperature promotes the narrowing of all intraconfigurational f-f transitions for the  $\text{Eu}^{3+}$  ions, due to the structural changes. In addition, all samples present good CIE (International Illumination Committee) chromaticity coordinates when excited in the UV (275 and 394 nm), blue (465 nm) and green (525 nm) radiation.

**Keywords:** non-hydrolytic sol-gel route, niobia, red phosphor, luminescence

### Introduction

Currently, solid-state white light emitters (LEDs) are considered the next generation of solid-state light sources. Because LEDs offer advantages such as longer lifetime and low energy consumption, they constitute potential replacements for incandescent and fluorescent light bulbs.<sup>1,2</sup> Bearing in mind that illumination consumes about 33% of all the generated energy, the development of energy-saving systems has become fundamental from a technological standpoint.<sup>3</sup>

Ultraviolet (UV) radiation provides high excitation energy, so a new strategy to obtain white light relies on the use of near UV radiation (ca. 400 nm) by LEDs coated with blue/green/red luminophores.<sup>4</sup> An ultraviolet light emitting diode composed of indium gallium nitride (InGaN) or gallium nitride (GaN) present a high light emission efficiency in the light emission wavelengths from

370 nm to 410 nm, and particularly, has the highest light emission efficiency at wavelengths around 390 nm.<sup>5</sup> Yttrium oxysulfide doped with  $\text{Eu}^{3+}$  ( $\text{Y}_2\text{O}_2\text{S}:\text{Eu}^{3+}$ ) is the red-light luminophore that is commercially available at present; however, it is less efficient than luminophores that emit blue and green light, has shorter lifetime under UV radiation, and is unstable because it releases hydrogen sulfide.<sup>6-9</sup> In this context, achieving novel and stable luminophores that can emit intense red light, exhibits excitation in the near UV region, and presents CIE (International Illumination Committee) chromaticity coordinates that meet the demands of the National Television Standard Committee (NTSC) is highly desirable.

To produce white light, the current phosphor materials based on near UV GaN-LEDs are  $\text{BaMgAl}_{10}\text{O}_{17}:\text{Eu}^{2+}$  (BAM) for blue,  $\text{ZnS}:(\text{Cu}^+, \text{Al}^{3+})$  for green, and  $\text{Y}_2\text{O}_2\text{S}:\text{Eu}^{3+}$  for red. However, compared with the blue and green phosphors, the efficiency of  $\text{Y}_2\text{O}_2\text{S}:\text{Eu}^{3+}$  is about eight times lower and a mixture containing 10% blue, 10% green and 80% red is necessary to obtain appreciable color

\*e-mail: lucas.rocha@unifran.edu.br

rendering.<sup>2</sup> Therefore, it is mandatory that scientists design new processes and search for novel materials to synthesize stable luminophores that can efficiently absorb near UV radiation while emitting red light. In this sense, niobium oxide doped with  $\text{La}^{3+}$  and  $\text{Eu}^{3+}$  has emerged as a promising material for multifunctional applications.

$\text{Nb}_2\text{O}_5$  is transparent over a wide range of wavelengths (0.35–9.0  $\mu\text{m}$ ), it has a wide band-gap (3.6 eV), it is stable under near UV radiation, it has a relatively low cut-off phonon energy (900  $\text{cm}^{-1}$ ), high refractive index (2.4), high permittivity (29 to 200 depending of the crystalline phase) and undergoes polymorphic transformations induced by treatment temperature.<sup>10–13</sup> All these properties enhance the optical features of rare earth ions, since efficient radiative emission output requires a relatively high refractive index and a low nonradioactive decay for excited states. The amorphous niobium oxide (V) begins to crystallize in a low-temperature form called the (T) form or  $\gamma$ -phase (orthorhombic, space group: Pbam) at about 500 °C. Crystallization occurs more rapidly at higher temperatures until about 800 °C, where upon a transition to a medium-temperature (M) form or  $\beta$ -phase (monoclinic, space group: I4/mmm). This transition continues more rapidly at higher temperatures and heating for 4 h at 1000 °C brings about a complete conversion. At even higher temperatures, a third transformation to a high-temperature (H) form or  $\alpha$ -phase (monoclinic, space group: P2/m) is observed. These polymorphic transitions take place slowly, at temperatures which are not well-defined, and are irreversible.<sup>14–16</sup>

Luminescent materials can absorb light from diverse sources and emit radiative electromagnetic energy in the visible, ultraviolet, and infrared regions.<sup>17</sup> Among the various methodologies that are available to synthesize luminophores, the non-hydrolytic sol-gel process stands out as one of the most advantageous: it yields highly pure products (the metallic oxides originate *in situ*) with fewer pores; occurs at relatively low temperatures; allows for incorporation of organic species, to give more homogeneous hybrid materials; and is easier to reproduce.<sup>18</sup>

In the traditional sol-gel process, the water molecules within the  $\text{Eu}^{3+}$  ion coordination sphere contribute to a non-radiative decay, which has increased the interest in alternative low-temperature processes that take place in the absence of water.<sup>19,20</sup> The non-hydrolytic sol-gel route is a versatile way to prepare inorganic oxides<sup>18</sup> during which non-hydrolytic condensation reactions furnish oxides and hybrid organic-inorganic materials; the oxo bonds originate from oxygen atoms of donors other than water.<sup>20</sup> This route provides strict control of stoichiometry, powder morphology, and phase purity; cations are distributed all over the polymeric structure. Thermal treatment at high

temperatures (from 400 °C) releases organic matter and produces well-ordered crystallites, which is important when one wishes to obtain high crystallinity and controlled distribution of the constituents within the crystalline network. The non-hydrolytic sol-gel process dismisses the need for solvents and may reduce or eliminate the formation of residual metal-OH groups.<sup>21</sup>

It is known that particle morphology and size affect the luminescent properties of  $\text{Nb}_2\text{O}_5$  matrices; that is, the features of the  $\text{Nb}_2\text{O}_5$  material depend on the methodology used to prepare the solid. Authors have employed countless methodologies to obtain  $\text{Nb}_2\text{O}_5$  matrixes, like sol-gel,<sup>10,11</sup> Pechini,<sup>22,23</sup> chemical transport,<sup>14</sup> hydrothermal route<sup>24,25</sup> and polymerized complexes.<sup>26</sup> Nevertheless, to date there are no reports on the use of the non-hydrolytic sol-gel technique to prepare these materials.

Thus, the present study employed the non-hydrolytic sol-gel route to prepare  $\text{Nb}_2\text{O}_5:\text{La}^{3+},\text{Eu}^{3+}$  matrixes at  $\text{Nb}_2\text{O}_5:\text{La}^{3+}_{(1.0\%x\%)}\text{Eu}^{3+}_{(x\%)}$  stoichiometric ratios, where  $x = 0.1$  and 0.3 mol%, to obtain red phosphors with a wide excitation range and adequate CIE chromaticity coordinates. The samples underwent thermal treatment at 550, 750, 900, and 1200 °C, for 4 h, followed by investigation of their luminescent properties.

## Experimental

All the solvents and reagents were of commercial grades (Merck and Sigma-Aldrich) unless otherwise stated.  $\text{NbCl}_5$  was donated by Companhia Brasileira de Metalurgia e Mineração (CBMM).

### Preparation of $\text{Nb}_2\text{O}_5:\text{La}^{3+}_{(1\%-x\%)}\text{Eu}^{3+}_{(x\%)}$

The preparation of the gel was carried out in oven-dried glassware. The material was synthesized via modification of the method described by Acosta *et al.*<sup>27</sup> Niobium pentachloride ( $\text{NbCl}_5$ , 5.55 mmol) was previously suspended in 5 mL of dry dichloromethane and 50 mL of ethanol; it was then reacted in the presence of lanthanum chloride ( $\text{LaCl}_3$ ,  $5.55 \times 10^{-2}$  mmol) under reflux at 110 °C, under argon atmosphere. For the samples doped with  $\text{Eu}^{3+}$  ions, an amount of europium chloride ( $\text{EuCl}_3$ ,  $5.55 \times 10^{-3}$  or  $1.66 \times 10^{-2}$  mmol) was added in the precursor solution. The condenser was placed in a thermostatic bath at  $-5$  °C. The gel was formed after 4 h of reaction; after 0.5 h, a solid material started to precipitate. After reflux, the mixture was cooled and aged overnight in the mother liquor, at room temperature. The solvent was removed under vacuum, and the solid was dried at 100 °C. The powders were annealed at 550, 750, 900, and 1200 °C for 4 h.

## Characterization

X-ray diffraction (XRD) was performed at room temperature using a Rigaku Geigerflex D/max-c diffractometer with monochromated  $\text{CuK}\alpha$  radiation ( $\lambda = 1.54 \text{ \AA}$ ). Diffractograms were recorded in the  $2\theta$  range from  $10$  to  $80^\circ$  at a resolution of  $0.05^\circ$ . Raman spectra of the materials were obtained in the Raman spectrometer Horiba Jobin Yvon model LabRAM HR 800, operating with a He-Ne laser at  $632.81 \text{ nm}$  equipped with a charged couple device (CCD) camera model DU420A-OE-325 from the same manufacturer. The spectrum was obtained in the region from  $100$  to  $4000 \text{ cm}^{-1}$  with a hole of  $100 \text{ }\mu\text{m}$  and length of  $5$  to  $30$  cycles. Photoluminescence data were obtained at room temperature, under continuous Xe lamp ( $450 \text{ W}$ ) excitation in a Horiba Jobin Yvon Fluorolog-3 spectrofluorimeter equipped with an excitation and emission double monochromator and a photomultiplier R 928 Hamamatsu. The emission was collected at  $90^\circ$  from the excitation beam. The slits were placed at  $2.0$  and  $0.5 \text{ nm}$  for excitation and emission, respectively; the bandpass was  $0.5 \text{ nm}$ , and the integration time was  $0.5 \text{ ms}$ . G1227 emission filters were employed (transmittance  $100\%$  for  $\lambda > 450 \text{ nm}$ ). The decay curves were acquired using a phosphorimeter accessory equipped with a Xe Lamp ( $5 \text{ J per pulse}$ ). Particle morphology was investigated by scanning electron microscopy (SEM) on a Shimadzu microscope model VEGA 3 SB.

## Results and Discussion

Figure 1 shows the XRD patterns of the samples sintered at different temperatures. Samples without thermal treatment do not display any peaks. Addition of increasing, but small amounts of the dopant  $\text{Eu}^{3+}$  does not shift the diffraction peaks, because the unit cell varies within the detection limit of the instrument. Samples sintered at  $550^\circ\text{C}$  present peaks indexed to the (T) phase of  $\text{Nb}_2\text{O}_5$  with an orthorhombic structure (JCPDS 30-873) and the  $\text{Nb}_3\text{O}_7\text{Cl}$  orthorhombic structure (JCPDS 73-295). Samples treated at  $750^\circ\text{C}$  contain  $\text{Nb}_2\text{O}_5$  polycrystalline phases indexed to the  $\text{Nb}_2\text{O}_5$  orthorhombic phase (JCPDS 30-873) and tetragonal structure (JCPDS 18-911). The crystalline (M) phase of the  $\text{Nb}_2\text{O}_5$  monoclinic structure (JCPDS 15-166) and the  $\text{La}_2\text{Nb}_{10}\text{O}_{28}$  orthorhombic phase (JCPDS 20-547) appear after sintering at  $900^\circ\text{C}$ . After the thermal treatment at  $1200^\circ\text{C}$ , a totally crystalline (H) phase indexed to the  $\text{Nb}_2\text{O}_5$  monoclinic structure (JCPDS 37-1468) and the  $\text{La}_2\text{Nb}_{10}\text{O}_{28}$  orthorhombic phase (JCPDS 20-547) were identified.

Figure 2 illustrates the Raman spectra of the samples after calcination at different temperatures. Untreated

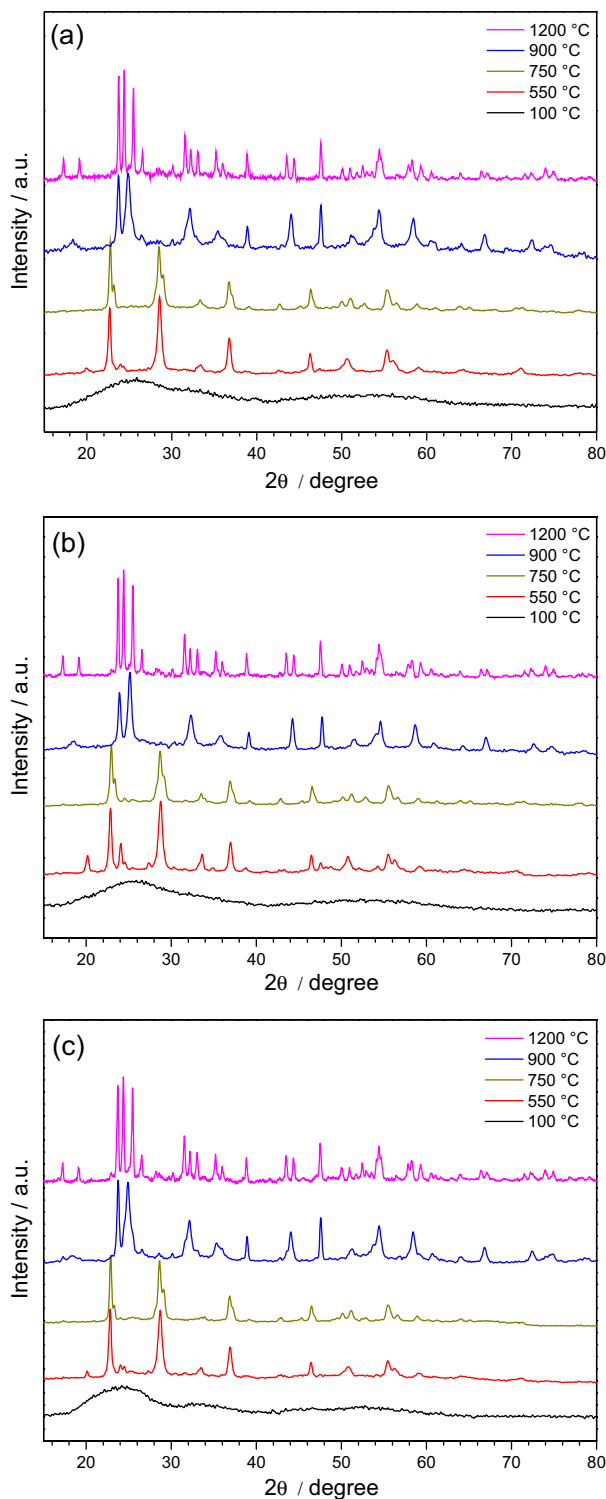


**Figure 1.** X-ray diffractograms of samples treated at different temperatures: (a)  $\text{Nb}_2\text{O}_5:\text{La}_{(1.0\%)}$ ; (b)  $\text{Nb}_2\text{O}_5:\text{La}_{(0.9\%)}\text{Eu}_{(0.1\%)}$ ; and (c)  $\text{Nb}_2\text{O}_5:\text{La}_{(0.7\%)}\text{Eu}_{(0.3\%)}$ .

samples display broad bands in the region of the  $60$ - $400$  and  $760$ - $1100 \text{ cm}^{-1}$  related to the precursor (Nb-Cl) and to the initial linkages between niobium and oxygen.<sup>11,28</sup> Confirming the data observed in X-ray diffraction, the results obtained by Raman spectroscopy confirmed the

polymorphism of niobia, which has many Nb–O polyhedra, being NbO<sub>6</sub> octahedrons, the most common presenting in the T, M and H phases in different degree of distortion. In the T phase, broad bands are always present due to the large number of hexa or hepta coordination of Nb *per* unit cell, which increased the distortion and the number of different sites occupied by niobium atoms. The M and H phases are very similar and less distorted.<sup>10,11</sup>

The samples calcined at 550 and 750 °C presented bands at around 130, 230 and 700 cm<sup>-1</sup> related to the optical vibration of Nb<sub>2</sub>O<sub>5</sub>, to the bending modes of the Nb–O–Nb linkage ( $\nu_4$ ) and to the vibrational mode related to the Nb–O symmetric stretching ( $\nu_1$ ). These vibrations are characteristic of the (T)-phase of Nb<sub>2</sub>O<sub>5</sub> as observed in the X-ray results and they are in agreement to the literature. A broad band between 560 and 790 cm<sup>-1</sup> is related to the vibrations of niobium polyhedrons in the (T)-phase of the Nb<sub>2</sub>O<sub>5</sub>. In addition, there is a weak shoulder around 890 cm<sup>-1</sup>, which corresponds to the symmetric stretching mode of surface Nb=O. For the samples annealed at higher temperature, an intense peak at 992 cm<sup>-1</sup> was assigned to the Nb–O symmetric stretching ( $\nu_1$ ) of the NbO<sub>6</sub> polyhedra, characteristic of the highly-ordered (M)- or (H)-phase.<sup>11,29</sup> There are low intensity bands at 895 and 847 cm<sup>-1</sup>, which correspond to the symmetric stretching mode of surface Nb=O and to the vibrational mode ( $\nu_1$ ) of the NbO<sub>4</sub> tetrahedron, once that one of the 28 Nb atoms in each unit cell is present in a tetrahedral site, which occurs at some block junctions. Several bands were also observed between 620 and 680 cm<sup>-1</sup>, which are related to the transverse optic modes in different types of octahedral arrangements.<sup>11,15,29</sup>

Low intensity bands at 350, 470 and 548 cm<sup>-1</sup> assigned to the mode ( $\nu_5$ ) are related to the block structures and the band at around 347 cm<sup>-1</sup> is ascribed to the corner-shared octahedra. The octahedral distortion provides the appearance of broad multiplet bands at 260–290 cm<sup>-1</sup> assigned to the infrared-active modes  $\nu_3$  and  $\nu_4$ ; the bands at 204 and 265 cm<sup>-1</sup> are characteristic of  $\nu_6$  modes and exist as a broad multiplet, also because of octahedral distortion.<sup>11,29</sup> As observed for the (T)-phase, the samples calcined at 900 and 1200 °C (M- and H-phase) also presented a band at around 120 cm<sup>-1</sup> but in this case, it probably arises from a more ordered structure. Finally, bands at 102 and 200 cm<sup>-1</sup> were assigned to the La–O vibrational mode,<sup>30,31</sup> due to the lanthanum niobate phase also detected by the X-ray diffraction.

SEM images (Figure 3) reveal some interesting morphologies. Non-calcined samples and samples sintered at 550 °C (Figures 4a<sub>1,2</sub>, 4b<sub>1,2</sub> and 4c<sub>1,2</sub>) present porous surface; surface particles are irregular. Samples treated at 750 °C (Figures 3a<sub>3</sub>, 3b<sub>3</sub> and 3c<sub>3</sub>) correspond to regular pellets with typical crystalline grain measuring around

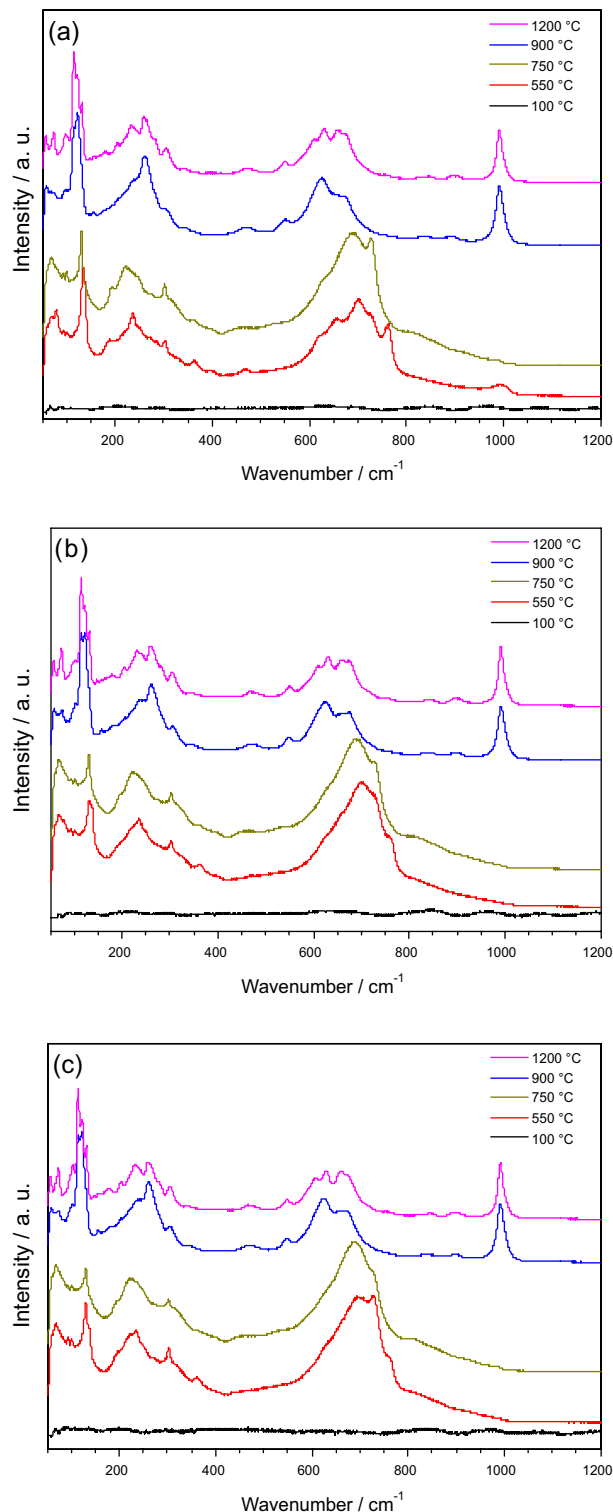


**Figure 2.** Raman spectra of samples treated at different temperatures: (a) Nb<sub>2</sub>O<sub>5</sub>:La<sub>1.0</sub>%; (b) Nb<sub>2</sub>O<sub>5</sub>:La<sub>0.9</sub>%Eu<sub>0.1</sub>%; and (c) Nb<sub>2</sub>O<sub>5</sub>:La<sub>0.7</sub>%Eu<sub>0.3</sub>%.

0.2–0.7 μm. Higher sintering temperature increases the crystalline grain size; indeed, the samples calcined at 900 and 1200 °C (Figures 3a<sub>4,5</sub>, 3b<sub>4,5</sub> and 3c<sub>4,5</sub>) have crystals with particle size around 0.7–5.0 μm; the pellets are arranged as sheets with a thickness estimated of around 60 nm

(Figure 4). This is in agreement with the values obtained by the Scherrer analysis,<sup>32</sup> which provided crystallite size of around 50 nm to the diffraction plane  $h\ k\ l\ (3\ 0\ 1)$  at  $2\theta = 17.25^\circ$  for the samples annealed at 1200 °C.

Figures 5 and 6 depict the luminescence spectra of the samples  $\text{Nb}_2\text{O}_5:\text{La}_{(0.9\%)}\text{Eu}_{(0.1\%)}$  and  $\text{Nb}_2\text{O}_5:\text{La}_{(0.7\%)}\text{Eu}_{(0.3\%)}$ , respectively, calcined at different temperatures. All the samples display a broad band at 275 nm in the excitation spectra ( $\lambda_{\text{em}}$ : 614 nm, Figures 5a and 6a), irrespective of the

thermal treatment temperature. This band was more intense for the  $\text{Nb}_2\text{O}_5:\text{La}_{(0.7\%)}\text{Eu}_{(0.3\%)}$  calcined at 750 and 900 °C (Figure 5a). Many literature papers describing niobium oxide doped with lanthanides have reported that the charge transfer (CT) band emerges in the excitation spectrum. Zhang *et al.*<sup>33</sup> detected the CT band at 280 nm for the  $\text{Li}_5(\text{La}_{2.7}\text{Eu}_{0.3})\text{Nb}_2\text{O}_{12}$  oxide obtained by solid-state reaction; the most intense band of the  $f \rightarrow f$  transition appeared at 463 nm and corresponded to the  ${}^7\text{F}_0 \rightarrow {}^5\text{D}_2$  transition.

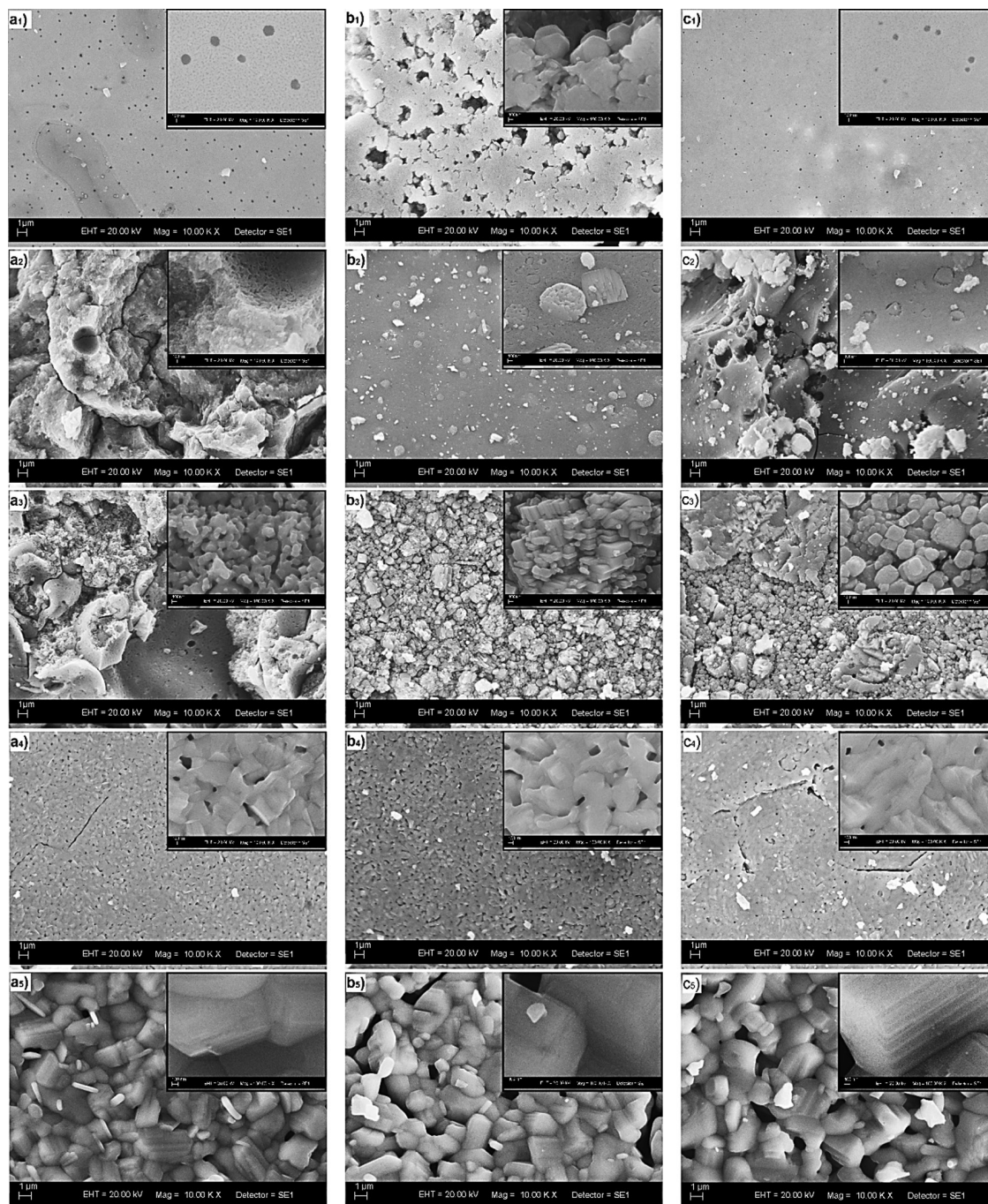


**Figure 3.** Scanning electron micrographs of samples (a)  $\text{Nb}_2\text{O}_5:\text{La}_{(1.0\%)}$ ; (b)  $\text{Nb}_2\text{O}_5:\text{La}_{(0.9\%)}\text{Eu}_{(0.1\%)}$ ; and (c)  $\text{Nb}_2\text{O}_5:\text{La}_{(0.7\%)}\text{Eu}_{(0.3\%)}$ . The indexes 1-5 indicate the thermal treatment temperature of 100, 500, 750, 900, and 1200 °C, respectively.

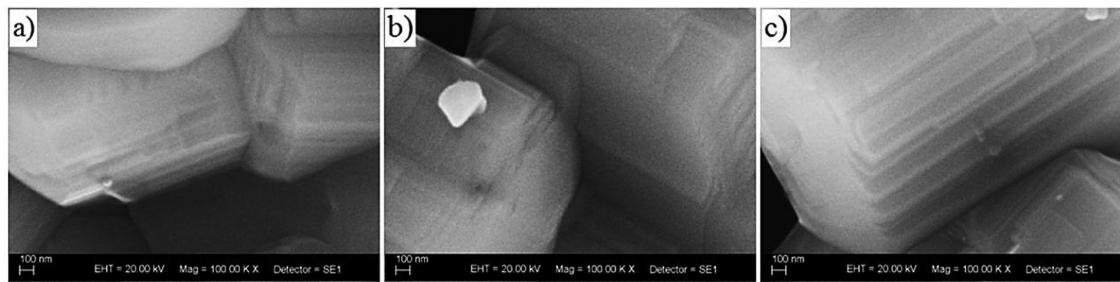


**Figure 4.** Scanning electron micrographs of samples: (a)  $\text{Nb}_2\text{O}_5\text{:La}_{(1.0\%)}$ ; (b)  $\text{Nb}_2\text{O}_5\text{:La}_{(0.9\%)}\text{Eu}_{(0.1\%)}$ ; and (c)  $\text{Nb}_2\text{O}_5\text{:La}_{(0.7\%)}\text{Eu}_{(0.3\%)}$  treated at 1200 °C.

The  $(\text{La}_{0.99}\text{Eu}_{0.01})\text{NbO}_4\text{:Eu}^{3+}$  matrix prepared by spray pyrolysis method display a large CT band between 240 and 310 nm, ascribed to CT band.<sup>34</sup> The  $\text{YNbO}_4\text{-EuNbO}_4$  system produced via hydrothermal route also presented the CT band between 240 and 270 nm.<sup>35</sup> On the other hand, the nanocrystalline powder  $\text{Ln}^{3+}$  doped  $\text{Nb}_2\text{O}_5$  obtained by the Pechini methodology did not have a CT band.<sup>36</sup> In our work, we hypothesize that this band is related to the  $\text{La}_2\text{Nb}_{10}\text{O}_{28}$  micro-crystalline phase; which was assign to the charge CT band resulting from the 2p orbital of oxygen to empty 4f orbitals of  $\text{Eu}^{3+}$  ( $\text{Eu}^{3+} \rightarrow \text{O}^{2-}$ ), and to charge transfer from the ligand oxygen to the empty 4f orbital of the central niobium atom of the group  $\text{NbO}_4^{3-}$  ( $\text{Nb}^{5+} \rightarrow \text{O}^{2-}$ ).<sup>5,34,37</sup> This fact is in agreement with the results obtained by the X-ray diffraction, that reveled the presence of the  $\text{La}_2\text{Nb}_{10}\text{O}_{28}$  as a secondary phase in the niobia host. It is important to note that in several crystals, such as lithium niobate, strontium barium niobate, and barium sodium niobate, the location of the  $\text{Ln}^{3+}$  in the lattice is not obvious, as the trivalent lanthanide ions cannot easily replace the constitutional cations ( $\text{Li}^+$ ,  $\text{Na}^+$ ,  $\text{Sr}^{2+}$ ,  $\text{Ba}^{2+}$ ,  $\text{Nb}^{5+}$ ) due to clear size and/or charge mismatches. This location has been addressed by several studies where optical and/or structural techniques have been employed.<sup>22</sup> Nevertheless, it is still a matter of debate whether the  $\text{Ln}^{3+}$  can substitute for the smaller and higher charged  $\text{Nb}^{5+}$  cation in a crystalline lattice. Falcomer *et al.*<sup>22</sup> reported that pentavalent niobium ions can be substituted by trivalent lanthanide ions in crystalline niobates, but this substitution is accompanied by a strong disorder around the  $\text{Ln}^{3+}$  ions.

In the excitation spectrum, a transition is observed only if this level is efficient in populating the emitting level and thus in generating luminescence. If an energy level is absent it means that this level is not efficient in absorbing the excitation light and/or is not able in populating the emitting level.<sup>38</sup> Transitions within the  $^7\text{F}$  ground term are only observed for  $\text{Eu}^{3+}$  ions doped in inorganic matrices with low phonon energies, since these transitions are otherwise masked by the much stronger overtones and combination bands of the vibrations of the host matrix or ligands.<sup>38</sup>

The sharp lines in the 380-600 nm range correspond to  $\text{Eu}^{3+}$  intraconfigurational 4f-4f transitions in the host lattices; the main excitation bands at 394, 465, 525 and 532 nm refer to the  $\text{Eu}^{3+}$  transitions:  $^7\text{F}_0 \rightarrow ^5\text{L}_6$ ,  $^5\text{D}_2$ ,  $^5\text{D}_1$  and  $^7\text{F}_1 \rightarrow ^5\text{D}_1$ , respectively. As the  $^7\text{F}_0 \rightarrow ^5\text{D}_1$  is a magnetic dipole transition, its intensity does not change. However, the increase of the annealing temperature promotes an increase of crystallinity (from orthorhombic to monoclinic) changing the local site symmetries for the  $\text{Eu}^{3+}$  ions and that can provide some differences in the intensities of the others electric dipole transitions. Higher annealing temperatures promote a decrease of the relative intensity of the  $^7\text{F}_0 \rightarrow ^5\text{L}_6$  transition and favors the  $^7\text{F}_1 \rightarrow ^5\text{D}_1$  transitions.

The emission spectrum for both samples show different profiles depending of excitation wavelengths and annealing temperatures. The samples excited at CT band (275 nm) exhibit broad bands for all intraconfigurational f-f transitions of  $\text{Eu}^{3+}$  ions, as presented in Figures 5b and 6b. Similar profiles were observed for the samples annealed at 750 °C and 900 °C, which were different in comparison with the samples annealed at 550 °C and 1200 °C. These three different behaviors are explained by the different crystalline phase. All samples calcined at 550 °C present inhomogeneous broad bands for the  $^5\text{D}_0 \rightarrow ^7\text{F}_j$  ( $j = 0, 1, 2, 3$  and 4) due to the presence of many sites of symmetry, which are different to each other. As mentioned above, it is characteristic of (T) phase of niobia, that presents in its unit cell, eight of the Nb ions are present in distorted octahedra, while another eight Nb ions occupy pentagonal bipyramids. The remaining 0.8 Nb ion *per* unit cell is located in interstitial 9-coordinated sites in the unit cell.<sup>15</sup> The samples annealed at 750, 900 and 1200 °C presented a narrowing in the emission bands in comparison with the samples calcined at 550 °C. For the samples calcined at higher temperatures, the (M) and (H) phase of the  $\text{Nb}_2\text{O}_5$ , have a shear structure consisting of blocks of  $\text{NbO}_6$  octahedra ( $3 \times 4$  and  $3 \times 5$ ) that share corners with octahedra in their own block and edges with octahedra in other blocks. One of the 28 Nb atoms in each unit cell is present in a tetrahedral site, which occurs at some block junctions.<sup>15</sup> In addition, as the  $^5\text{D}_0 \rightarrow ^7\text{F}_4$  transition is also

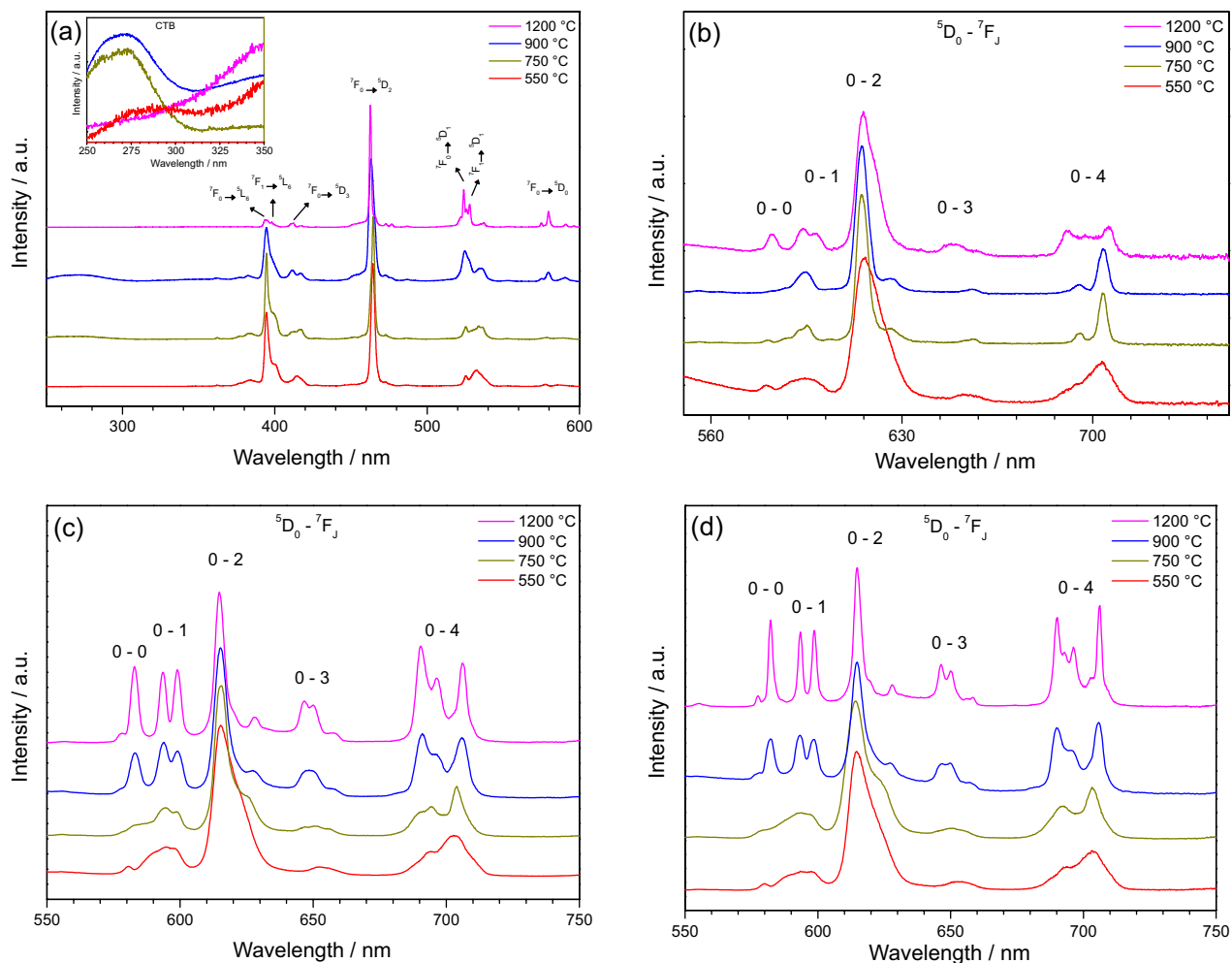


**Figure 5.** Luminescence spectra of the sample Nb<sub>2</sub>O<sub>5</sub>:La<sub>(0.9%)</sub>Eu<sub>(0.1%)</sub> calcined at different temperatures: (a) excitation spectra ( $\lambda_{em}$ : 614 nm); (b) emission spectra ( $\lambda_{exc}$ : 275 nm); (c) emission spectra ( $\lambda_{exc}$ : 394 nm); (d) emission spectra ( $\lambda_{exc}$ : 465 nm) and (e) emission spectra ( $\lambda_{exc}$ : 525 nm).

sensitive to the local symmetry, the structure changes can be observed by the variation of its intensity. The emission spectra (Figures 5a and 6a) excited at 275 nm for these samples present similar profiles to those already published in the literature,<sup>1,33,34,36</sup> which describe the preparation of niobates matrices doped with the Eu<sup>3+</sup> ions, suggesting that under CT band excitation, the majority emitting ions are located in the lanthanum niobate phase.

The presence of the  $^5D_0 \rightarrow ^7F_0$  transition is an indication that the Eu<sup>3+</sup> ion occupies a site with  $C_{nv}$ ,  $C_n$  or  $C_s$  symmetry.<sup>38,39</sup> In addition, this transition is also useful to confirming the presence of non-equivalent sites in a host structure, because due to the non-degeneracy of the  $^7F_0$  and  $^5D_0$  levels, it is expected only one peak for a single site or species. The observation of more than one peak indicates that more than one site or species is present. Slight differences between two sites can provide small energy differences between the two different peaks in the  $^5D_0 \rightarrow ^7F_0$  region, and the presence of more than one site for the Eu<sup>3+</sup> ions is verified by the asymmetric shape of

this transition or as a shoulder.<sup>38</sup> Although this transition is strictly forbidden according to the standard Judd-Ofelt theory, it occurs due to J-mixing. J is the total angular quantum number and it indicates the relative orientation of the spin and the orbital momenta. The J quantum numbers are well defined in the free Eu<sup>3+</sup> ion, but J-mixing is due to the crystal-field perturbation which causes a mixing of the wave functions of terms with different J values.<sup>38</sup>

The emission spectra excited directly in the Eu<sup>3+</sup> ions transitions (Figures 5c-e and 6c-e) prompts the appearance of bands characteristic of the transition from the excited state  $^5D_0$  to the fundamental level  $^7F_J$  ( $J = 0, 1, 2, 3, \text{ and } 4$ ). The emission profiles for the samples excited at 394, 465 and 525 nm presented great differences in comparison to those excited at 275 nm, suggesting the existence of different local sites symmetry for the Eu<sup>3+</sup> ions. As the lanthanum ions are present in low concentration in comparison with the niobium ions, the majority of Eu<sup>3+</sup> ions are most probably located in the niobia phase. For these samples, it was observed a narrowing of the bands

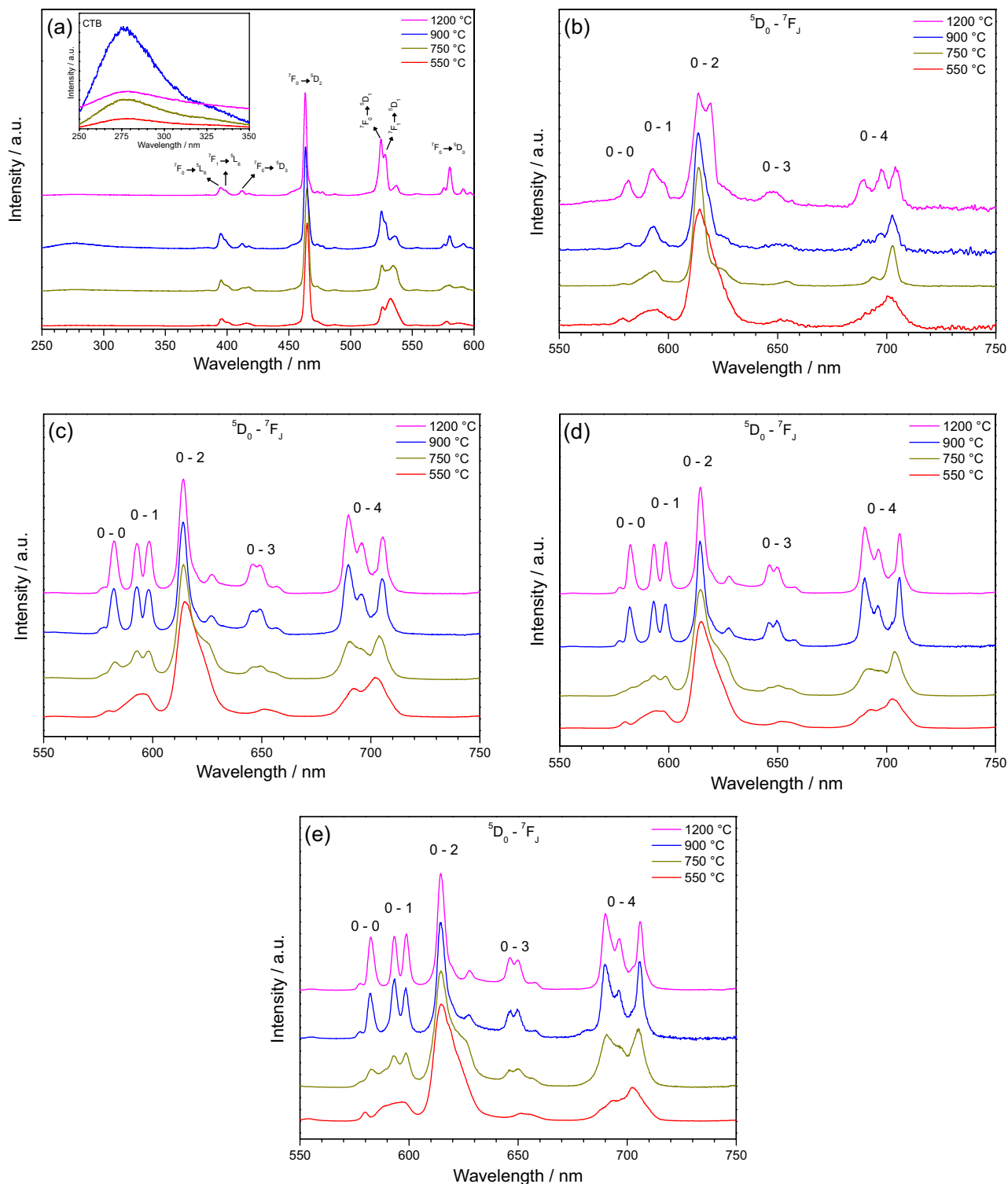


**Figure 6.** Luminescence spectra of the sample  $\text{Nb}_2\text{O}_5:\text{La}_{(0.7\%)}\text{Eu}_{(0.3\%)}$  calcined at different temperatures: (a) excitation spectra ( $\lambda_{\text{em}}: 614 \text{ nm}$ ), (b) emission spectra ( $\lambda_{\text{exc}}: 275 \text{ nm}$ ), (c) emission spectra ( $\lambda_{\text{exc}}: 394 \text{ nm}$ ), (d) emission spectra ( $\lambda_{\text{exc}}: 465 \text{ nm}$ ) and (e) emission spectra ( $\lambda_{\text{exc}}: 525 \text{ nm}$ ).

in function of the thermal treatment temperature. The samples calcined at 900 and 1200 °C presented two bands in the  ${}^5\text{D}_0 \rightarrow {}^7\text{F}_0$  transition region at 577.5 and 582.6 nm, evidencing that at least two active sites exist. This fact corroborates with the X-ray diffraction results, which show

distinct phases for the calcined samples. An increase of the  ${}^5\text{D}_0 \rightarrow {}^7\text{F}_0$  transition's intensity was observed for the samples calcined at higher temperatures due to an increase system's crystallinity. Similar results were published for  $\text{Sr}_2\text{TiO}_4:\text{Eu}^{3+}$ ,  $\text{Ln}_2\text{O}_2\text{SO}_4$  ( $\text{Ln} = \text{La}, \text{Gd}, \text{Y}$ ),  $\text{Gd}_2\text{O}_3$  and

Y<sub>2</sub>O<sub>3</sub> materials.<sup>38,40-42</sup> In these cases, the high intensity of the <sup>5</sup>D<sub>0</sub> → <sup>7</sup>F<sub>0</sub> transition was ascribed to ordered crystal structure, which leads to large linear terms in the crystal-field potential.<sup>38</sup>

The <sup>5</sup>D<sub>0</sub> → <sup>7</sup>F<sub>1</sub> transition directly reflects the crystal-field splitting of the <sup>7</sup>F<sub>1</sub> level. In a high symmetry such as, cubic or icosahedral crystal-fields, the <sup>7</sup>F<sub>1</sub> level is not split. In hexagonal or tetragonal crystal-fields, it is split into a non-degenerate and a twofold degenerate crystal-field level and in orthorhombic or lower symmetries, the total removal of crystal field degeneracies results in three sublevels for <sup>7</sup>F<sub>1</sub>.<sup>38</sup> The samples presented an increase of splitting for the <sup>5</sup>D<sub>0</sub> → <sup>7</sup>F<sub>1</sub>, indicating an increase of the local symmetry for the Eu<sup>3+</sup> ions.

The peak at 582.5 nm could in principle be assigned to the <sup>5</sup>D<sub>0</sub> → <sup>7</sup>F<sub>1</sub> transition or in our case, to the <sup>5</sup>D<sub>0</sub> → <sup>7</sup>F<sub>0</sub> transition. According to Antic-Fidancev, a correlation exists between the position of the <sup>5</sup>D<sub>0</sub> level of Eu<sup>3+</sup> and the position of the barycenter of the <sup>7</sup>F<sub>1</sub> manifold.<sup>43</sup> If the <sup>5</sup>D<sub>0</sub> level is at 17300 cm<sup>-1</sup> (578.0 nm), the barycenter of the <sup>7</sup>F<sub>1</sub> manifold is expected at about 400 cm<sup>-1</sup>, which is not in agreement with our experimental values (17316 cm<sup>-1</sup> and 240 cm<sup>-1</sup>, respectively).

The most intense line appears at 614 nm and corresponds to the forced Eu<sup>3+</sup> <sup>5</sup>D<sub>0</sub> → <sup>7</sup>F<sub>2</sub> electric transition, indicating the absence of inversion symmetry in the sites occupied by Eu<sup>3+</sup> ions.<sup>5</sup> All samples presented a narrowing and an unfolding of the <sup>5</sup>D<sub>0</sub> → <sup>7</sup>F<sub>2</sub> transition with an increase of the annealed temperature. That fact is related to the changing of structure crystal as indicated by the results discussed heretofore. Only Nb<sub>2</sub>O<sub>5</sub>:La<sub>(0.7%)</sub>Eu<sub>(0.3%)</sub> treated at 1200 °C and excited at 275 nm presented unfolding of this transition around 619 nm, probably as a consequence of higher occupation of different active sites by the emitting ion, due to its larger concentration in the matrix.

The ratio between the integrated intensities of these two transitions, I<sub>0,2</sub>/I<sub>0,1</sub>, functions as a probe of the local cation surroundings. The ratio values decrease as a function of the thermal treatment temperature for both Nb<sub>2</sub>O<sub>5</sub>:La<sub>(0.9%)</sub>Eu<sub>(0.1%)</sub> and Nb<sub>2</sub>O<sub>5</sub>:La<sub>(0.7%)</sub>Eu<sub>(0.3%)</sub>. For an example, the values found for the Nb<sub>2</sub>O<sub>5</sub>:La<sub>(0.9%)</sub>Eu<sub>(0.1%)</sub> sample excited at 465 nm were 6.18, 4.39, 2.64 and 2.02 for calcination temperatures of 550, 750, 900 and 1200 °C, respectively; and for the Nb<sub>2</sub>O<sub>5</sub>:La<sub>(0.7%)</sub>Eu<sub>(0.3%)</sub> sample excited at 465 nm, the values ratio were 5.63, 4.72, 2.46 and 2.08 for calcination temperatures of 550, 750, 900, and 1200 °C, respectively. The ratio between the intensities of the <sup>5</sup>D<sub>0</sub> → <sup>7</sup>F<sub>2</sub> and <sup>5</sup>D<sub>0</sub> → <sup>7</sup>F<sub>1</sub> transitions varies as a function of the thermal treatment temperature, showing that Eu<sup>3+</sup> exists in a distorted (or asymmetric) cationic environment in

the samples calcined at 550 and 750 °C. At higher treatment temperatures, the Eu<sup>3+</sup> ions are preferentially located close to more crystalline and symmetric regions.

The <sup>5</sup>D<sub>0</sub> → <sup>7</sup>F<sub>3</sub> transition presented a similar behavior to the <sup>5</sup>D<sub>0</sub> → <sup>7</sup>F<sub>0</sub> transition, with an increase of intensity in function of the thermal treatment for all samples. In general the <sup>5</sup>D<sub>0</sub> → <sup>7</sup>F<sub>3</sub> transition is very weak, because it is forbidden according to the Judd-Ofelt theory, and as the <sup>5</sup>D<sub>0</sub> → <sup>7</sup>F<sub>0</sub> transition, the <sup>5</sup>D<sub>0</sub> → <sup>7</sup>F<sub>3</sub> transition can only gain intensity via J-mixing.<sup>38</sup> The increase of its intensity for the higher temperature annealed samples indicates an increase of J-mixing and crystal-field perturbation, caused by the structural changes.

Other indicative of structural changes can be observed by the variation of the <sup>5</sup>D<sub>0</sub> → <sup>7</sup>F<sub>4</sub> transition. The intensity of this transition is determined not only by symmetry factors, but also by the chemical composition of the host matrix.<sup>38</sup> As can be observed in the emission spectrum, the <sup>5</sup>D<sub>0</sub> → <sup>7</sup>F<sub>4</sub> transition presented different profiles with an increase of the annealing temperature and the europium concentration. Comparing the samples calcined at different temperatures, it was observed an increase of intensity, a narrowing and an higher unfolding for this transition, caused by the structural changes in the matrix. These structural changes allowed to obtain a deep-red emitting phosphor (ca. 700 nm). This fact is important because if a larger color gamut is required, e.g., for high-quality TV, monitors for design applications, etc., the primaries, i.e., the light transmitted by the blue, green, and red sections of the color filter, must be more separated from each other.<sup>44</sup> In addition, slight changes on the intensity and split of this transition were also observed with an increase of europium concentration, as showed in the emission spectrum for the samples annealed at 900 and 1200 °C in Figures 5b-e and 6b-e.

Figure 7 brings the decay curves for the emission from the <sup>5</sup>D<sub>0</sub> states for both samples, treated at different temperatures. Table 1 lists the excited state lifetimes. The decay does not follow a simple exponential law, confirming the distribution of symmetry sites for the Eu<sup>3+</sup> ion along the sample and providing a mean lifetime (τ<sub>exp</sub>). In general, the Eu<sup>3+</sup> ion lifetime increases in function of the thermal treatment temperature, which causes an increase on the structural crystallinity of the host as also confirmed by the X-rays diffraction and by the narrowing of the intraconfigurational f-f transitions of the Eu<sup>3+</sup> ions in the emission spectrum.

The emission spectra allowed us to calculate the spontaneous emission coefficient (A<sub>RAD</sub>), the radiative lifetime (τ<sub>RAD</sub>), the quantum efficiency (q), and the Judd-Ofelt (Ω<sub>2</sub>, Ω<sub>4</sub>) parameters (Table 1). The <sup>5</sup>D<sub>0</sub> → <sup>7</sup>F<sub>1</sub> transition is purely magnetically dipolar, and its radiative

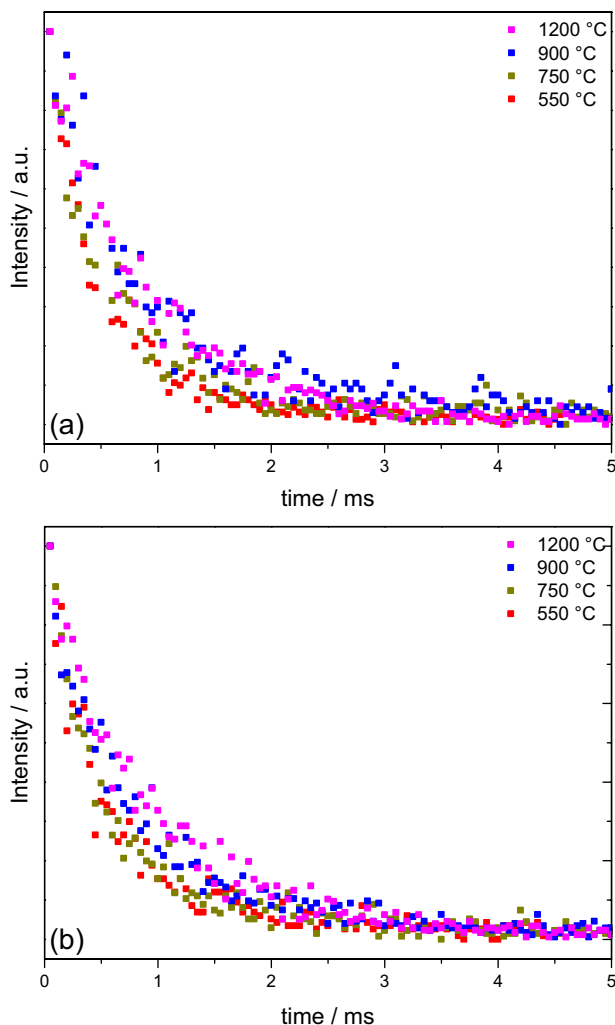


**Figure 7.** Decay curves for the  $\text{Eu}^{3+}$  ion in the matrixes (a)  $\text{Nb}_2\text{O}_5:\text{La}_{(0.9\%)}\text{Eu}_{(0.1\%)}$  and (b)  $\text{Nb}_2\text{O}_5:\text{La}_{(0.7\%)}\text{Eu}_{(0.3\%)}$  treated at different temperatures.

rate does not depend on the local field imposed by the environment. The relation  $A_{0-\lambda} = A_{0-1}(S_{0-\lambda}/S_{0-1})(\sigma_\lambda/\sigma_1)$ , where  $S_{0-\lambda}$  is the area under the curve related to the  ${}^5\text{D}_0 \rightarrow {}^7\text{F}_\lambda$  transition obtained from the spectral data, and  $\sigma_\lambda$  is the energy barycenter of the  $0-\lambda$  transition, furnishes the  $A_{0-\lambda}$  values. Here, we assumed that  $A_{0-1} = 50 \text{ s}^{-1}$ , and

**Table 1.** Judd-Ofelt intensity parameters ( $\Omega_2, \Omega_4$ ), probability of spontaneous Einstein emission ( $A_{\text{RAD}}$ ), radiative and experimental lifetimes ( $\tau_{\text{RAD}}, \tau_{\text{EXP}}$ ), and quantum efficiency ( $q$ ) of the calcined  $\text{Nb}_2\text{O}_5:\text{La}_{(0.9\%)}\text{Eu}_{(0.1\%)}$  and  $\text{Nb}_2\text{O}_5:\text{La}_{(0.7\%)}\text{Eu}_{(0.3\%)}$  samples

Sample	Temperature / °C	$\Omega_2 / (10^{-20} \text{ cm}^2)$	$\Omega_4 / (10^{-20} \text{ cm}^2)$	$A_{\text{RAD}} / \text{ms}^{-1}$	$\tau_{\text{RAD}} / \text{ms}$	$\tau_{\text{EXP}} / \text{ms}$	$q$
$\text{Nb}_2\text{O}_5:\text{La}_{(0.9\%)}\text{Eu}_{(0.1\%)}$	550	$6.2 \pm 0.3$	$5.7 \pm 0.3$	$0.54 \pm 0.03$	$1.85 \pm 0.09$	$0.66 \pm 0.07$	$0.36 \pm 0.05$
	750	$4.4 \pm 0.2$	$4.7 \pm 0.2$	$0.42 \pm 0.02$	$2.38 \pm 0.1$	$0.75 \pm 0.08$	$0.32 \pm 0.05$
	900	$2.6 \pm 0.1$	$5.8 \pm 0.3$	$0.39 \pm 0.02$	$2.59 \pm 0.1$	$0.94 \pm 0.09$	$0.36 \pm 0.05$
	1200	$2.0 \pm 0.1$	$6.1 \pm 0.3$	$0.38 \pm 0.02$	$2.64 \pm 0.1$	$0.93 \pm 0.09$	$0.35 \pm 0.05$
$\text{Nb}_2\text{O}_5:\text{La}_{(0.7\%)}\text{Eu}_{(0.3\%)}$	550	$5.6 \pm 0.3$	$4.8 \pm 0.2$	$0.49 \pm 0.02$	$2.05 \pm 0.1$	$0.70 \pm 0.07$	$0.34 \pm 0.05$
	750	$4.7 \pm 0.2$	$6.0 \pm 0.3$	$0.48 \pm 0.02$	$2.08 \pm 0.1$	$0.71 \pm 0.07$	$0.34 \pm 0.05$
	900	$2.4 \pm 0.1$	$6.8 \pm 0.3$	$0.41 \pm 0.02$	$2.41 \pm 0.1$	$0.96 \pm 0.10$	$0.40 \pm 0.06$
	1200	$2.1 \pm 0.1$	$5.3 \pm 0.3$	$0.37 \pm 0.02$	$2.71 \pm 0.1$	$0.97 \pm 0.10$	$0.36 \pm 0.05$

that  ${}^5\text{D}_0 \rightarrow {}^7\text{F}_{5,6}$  have negligible intensities. Although the calculations of radiative rates were based in lanthanide complexes in solutions, they have been used for lanthanides doped in solid state matrices as a form to evaluate its luminescent properties.<sup>45-48</sup> The details of these calculation were given by Werts *et al.*<sup>49</sup> The mean lifetime was calculated using the equation  $\langle \tau \rangle = \sum \alpha_i \cdot \tau_i / \sum \alpha_i$ ;  $\alpha$  and  $\tau$  represent the pre-exponential factor or amplitude and lifetime of the decay components, respectively.<sup>50</sup>

All the samples have presented similar  $q$  values between 30 and 40%. Rising calcination temperatures reduce  $A_{\text{RAD}}$  and  $\Omega_2$ . Reisfeld and Jørgensen<sup>51</sup> consider that  $\Omega_2$  is a useful parameter, because it is sensitive to the local symmetry of the ligand field and bond covalency. The value of  $\Omega_2$  increases as the local symmetry of the ligand field decreases and the bond covalency increases. The  $\Omega_4$  and  $\Omega_6$  are related to the viscosity and rigidity of the host medium in which the ions are situated, but there is no theoretical prediction for this sensibility to macroscopic properties.<sup>51,52</sup>

The increase of the annealed temperatures promoted a decrease of the  $\Omega_2$  values for the samples, indicating an increase of the local symmetry for the  $\text{Eu}^{3+}$  ions.<sup>53</sup> This fact corroborates with the results obtained by the X-ray diffraction that shows a higher crystallinity phases for the samples calcined at higher temperatures. In addition, these structural changes were also observed in the emission spectra of the  $\text{Eu}^{3+}$  ions in different annealed samples. However, the low  $\Omega_2$  and  $\Omega_4$  values obtained suggest that a weakly polarizable and rigid chemical environment surrounds  $\text{Eu}^{3+}$ .<sup>53</sup>

The stronger transition at 614 nm favors saturated CIE chromaticity. We generated chromaticity coordinates for the  $\text{Nb}_2\text{O}_5:\text{La}_{(0.9\%)}\text{Eu}_{(0.1\%)}$  and  $\text{Nb}_2\text{O}_5:\text{La}_{(0.7\%)}\text{Eu}_{(0.3\%)}$  samples using the software Spectra Lux 2.0<sup>54</sup> and the respective emission spectra recorded at room temperature (Tables 2 and 3). The CIE chromaticity coordinates of all the samples excited at 465 nm lie above the NTSC standard values ( $x = 0.670$  and  $y = 0.330$ ).<sup>5</sup> Moreover, the full width at

**Table 2.** Chromaticity coordinates and FWHM of the Eu<sup>3+</sup><sup>5</sup>D<sub>0</sub> → <sup>7</sup>F<sub>2</sub> transition in calcined Nb<sub>2</sub>O<sub>5</sub>:La<sub>(0.9%)</sub>Eu<sub>(0.1%)</sub> and Nb<sub>2</sub>O<sub>5</sub>:La<sub>(0.7%)</sub>Eu<sub>(0.3%)</sub> samples excited at 275 and 394 nm

Sample	Temperature / °C	$\lambda_{exc}^a$ : 275 nm			$\lambda_{exc}^a$ : 394 nm		
		CIE		FWHM <sup>b</sup> / nm	CIE		FWHM <sup>b</sup> / nm
		x	y		x	y	
Nb <sub>2</sub> O <sub>5</sub> :La <sub>(0.90%)</sub> Eu <sub>(0.1)</sub>	550	0.666	0.333	12.0	0.676	0.322	12.4
	750	0.660	0.338	5.2	0.662	0.336	6.3
	900	0.669	0.329	6.0	0.670	0.329	5.7
	1200	0.658	0.341	9.0	0.680	0.318	4.4
Nb <sub>2</sub> O <sub>5</sub> :La <sub>(0.7%)</sub> Eu <sub>(0.3)</sub>	550	0.681	0.318	12.0	0.683	0.316	13.8
	750	0.657	0.342	6.2	0.678	0.321	7.7
	900	0.651	0.347	5.0	0.671	0.327	4.8
	1200	0.649	0.350	9.0	0.676	0.322	5.2

<sup>a</sup>Excitation spectra; <sup>b</sup>full width at half maximum.

**Table 3.** Chromaticity coordinates, quantum efficiency (q) and FWHM of the Eu<sup>3+</sup><sup>5</sup>D<sub>0</sub> → <sup>7</sup>F<sub>2</sub> transition in calcined Nb<sub>2</sub>O<sub>5</sub>:La<sub>(0.9%)</sub>Eu<sub>(0.1%)</sub> and Nb<sub>2</sub>O<sub>5</sub>:La<sub>(0.7%)</sub>Eu<sub>(0.3%)</sub> samples excited at 465 and 525 nm

Sample	Temperature / °C	$\lambda_{exc}^a$ : 465 nm			$\lambda_{exc}^a$ : 525 nm		
		CIE		FWHM <sup>a</sup> / nm	CIE		FWHM <sup>b</sup> / nm
		x	y		x	y	
Nb <sub>2</sub> O <sub>5</sub> :La <sub>(0.9%)</sub> Eu <sub>(0.1%)</sub>	550	0.680	0.319	10.5	0.671	0.328	13.5
	750	0.681	0.317	7.0	0.663	0.335	7.7
	900	0.678	0.321	5.0	0.662	0.337	6.0
	1200	0.682	0.317	3.5	0.660	0.339	3.5
Nb <sub>2</sub> O <sub>5</sub> :La <sub>(0.7%)</sub> Eu <sub>(0.3%)</sub>	550	0.685	0.313	12.5	0.683	0.316	13.5
	750	0.687	0.312	11.3	0.689	0.309	9.1
	900	0.683	0.316	5.0	0.682	0.316	5.0
	1200	0.682	0.317	4.0	0.682	0.316	4.5

<sup>a</sup>Full width at half maximum.

half maximum (FWHM) values diminish with increasing treatment temperature: Nb<sub>2</sub>O<sub>5</sub>:La<sub>(0.9%)</sub>Eu<sub>(0.1%)</sub> calcined at 1200 °C affords the lowest value among the investigated samples, 3.5 nm.

## Conclusions

In this work, we prepared Nb<sub>2</sub>O<sub>5</sub>:La<sup>3+</sup>,Eu<sup>3+</sup> phosphors by the non-hydrolytic sol-gel process. The SEM images revealed that particles resembled pellets arranged into sheets with thickness of ca. 60 nm and the samples annealed above 900 °C elicited a totally crystalline monoclinic phase. On the contrary of Y<sub>2</sub>O<sub>2</sub>S:Eu<sup>3+</sup> which efficiently absorbs light at around 370 nm<sup>55,56</sup> the luminescence results shown that all samples presented a wide excitation reange, including the light emission region of a light emitting diode emitting UV (275, 394 nm), the blue (465 nm) and green (525 nm)

light. The CIE chromaticity coordinates were above the NTSC standard values. Hence, these two phosphors are promising red components for LED applications.

## Acknowledgments

The authors would like to deeply express our most sincere thanks to Jeannette Dexpert-Ghys (CEMES) for her profitable assistance and cooperation. The agencies CNPq, and CAPES (Brazilian research funding agencies), grant 2011/51858-0 Brazil-France cooperation program FAPESP-CNRS; 2011/09823-4 and 2012/11673-3 E.J.N.; 2011/15757-4 L.A.R.; São Paulo Research Foundation (FAPESP). The authors thank the Laboratory of Photonic Materials (Prof S. J. L. Ribeiro) for the use of the RAMAN spectrometer and CBMM (Companhia Brasileira de Metalurgia e Mineração) for donating NbCl<sub>5</sub>.

## References

- Huang, J.; Zhou, L.; Liang, Z.; Gong, F.; Han, J.; Wang, R.; *J. Rare Earths* **2010**, *28*, 356.
- Neeraj, S.; Kijima, N.; Cheetham, A. K.; *Chem. Phys. Lett.* **2004**, *387*, 2.
- Thejo Kalyani, N.; Dhoble, S. J.; *Renewable Sustainable Energy Rev.* **2012**, *16*, 2696.
- Wu, Z. C.; Shi, J. X.; Wang, J.; Gong, M. L.; Su, Q.; *J. Solid State Chem.* **2006**, *179*, 2356.
- Zhou, L.; Huang, J.; Gong, F.; Lan, Y.; Tong, Z.; Sun, J.; *J. Alloys Compd.* **2010**, *495*, 268.
- Ferrari, J. L.; Cebim, M. A.; Pires, A. M.; dos Santos, M. A. C.; Davolos, M. R.; *J. Solid State Chem.* **2010**, *183*, 2110.
- Kodaira, C. A.; Stefani, R.; Maia, A. S.; Felinto, M. C. F. C.; Brito, H. F.; *J. Lumin.* **2007**, *127*, 616.
- Pires, A. M.; Serra, O. A.; Davolos, M. R.; *J. Alloys Compd.* **2004**, *374*, 181.
- Kutty, T. R. N.; Nag, A.; *J. Mater. Chem.* **2003**, *13*, 2271.
- Aquino, F. T.; Ferrari, J. L.; Ribeiro, S. J. L.; Ferrier, A.; Goldner, P.; Gonçalves, R. R.; *Opt. Mater. (Amsterdam, Neth.)* **2013**, *35*, 387.
- Aquino, F. T.; Pereira, R. R.; Ferrari, J. L.; Ribeiro, S. J. L.; Ferrier, A.; Goldner, P.; Gonçalves, R. R.; *Mater. Chem. Phys.* **2014**, *147*, 751.
- Palatnikov, M.; Shcherbina, O.; Sidorov, N.; Skab, I.; Bormanis, K.; *Ukr. J. Phys. Opt.* **2012**, *13*, 207.
- Rooksby, H. P.; White, E. A. D.; *Acta Crystallogr.* **1963**, *16*, 888.
- Emmenegger, F. P.; Robinson, M. L. A.; *J. Phys. Chem. Solids* **1968**, *29*, 1673.
- Nowak, I.; Ziolk, M.; *Chem. Rev.* **1999**, *99*, 3603.
- Blanquart, T.; Niinistö, J.; Heikkilä, M.; Sajavaara, T.; Kukli, K.; Puukilainen, E.; Xu, C.; Hunks, W.; Ritala, M.; Leskelä, M.; *Chem. Mater.* **2012**, *24*, 975.
- Blasse, G.; Grabmaier, B. C.; *Luminescent Materials*; Springer: Berlin, 1994.
- Nassar, E. J.; Avila, L. R.; Pereira, P. F. S.; de Lima, O. J.; Rocha, L. A.; Mello, C.; Ciuffi, K. J.; Carlos, L. D.; *Quim. Nova* **2005**, *28*, 238.
- Ricci, G. P.; Rocha, Z. N.; Nakagaki, S.; Castro, K. A. D. F.; Crotti, A. E. M.; Calefi, P. S.; Nassar, E. J.; Ciuffi, K.; *Appl. Catal., A* **2010**, *389*, 147.
- Mutin, P. H.; Vioux, A.; *Chem. Mater.* **2009**, *21*, 582.
- Sommerdijk, N.; Wright, J. D.; *J. Sol-Gel Sci. Technol.* **1998**, *13*, 565.
- Falcomer, D.; Speghini, A.; Ibba, G.; Enzo, S.; Cannas, C.; Musinu, A.; Bettinelli, M.; *J. Nanomater.* **2007**, *2007*, DOI <http://dx.doi.org/10.1155/2007/94975>.
- Graça, M. P. F.; Meireles, A.; Nico, C.; Valente, M. A.; *J. Alloys Compd.* **2013**, *553*, 177.
- Luo, H.; Wei, M.; Wei, K.; *Mater. Chem. Phys.* **2010**, *120*, 6.
- Wei, M.; Wei, K.; Ichihara, M.; Zhou, H.; *Electrochem. Commun.* **2008**, *10*, 980.
- Bueno, P. R.; Faria, R. C.; Bulhões, L. O. S.; *Solid State Ionics* **2005**, *176*, 1175.
- Acosta, S.; Corriu, R. J. P.; Leclercq, D.; Lefèvre, P.; Mutin, P. H.; Vioux, A.; *J. Non-Cryst. Solids* **1994**, *170*, 234.
- Konings, R. J. M.; Booij, A. S.; *Vib. Spectrosc.* **1994**, *6*, 345.
- McConnell, A. A.; Anderson, J. S.; Rao, C. N. R.; *Spectrochim. Acta, Part A* **1976**, *32*, 1067.
- Boldish, S. I.; White, W. B.; *Spectrochim. Acta, Part A* **1979**, *35*, 1235.
- Weckhuysen, B. M.; *Phys. Chem. Chem. Phys.* **2003**, *5*, 4351.
- Burton, A. W.; Ong, K.; Rea, T.; Chan, I. Y.; *Microporous Mesoporous Mater.* **2009**, *117*, 75.
- Zhang, X.; Meng, F.; Wei, H.; Seo, H. J.; *Ceram. Int.* **2013**, *39*, 4063.
- Freiria, G. S.; Nassar, E. J.; Verelst, M.; Rocha, L. A.; *J. Lumin.* **2015**, DOI [dx.doi.org/10.1016/j.jlumin.2015.06.022](https://doi.org/10.1016/j.jlumin.2015.06.022).
- Hirano, M.; Dozono, H.; *Mater. Res. Bull.* **2014**, *50*, 213.
- Hsiao, Y. J.; Fang, T. H.; Chang, Y. S.; Chang, Y. H.; Liu, C. H.; Ji, L. W.; Jywe, W. Y.; *J. Lumin.* **2007**, *126*, 866.
- Mahesh, S. K.; Rao, P. P.; Francis, T. L.; Reshmi, V. R.; Koshy, P.; *Mater. Lett.* **2014**, *120*, 115.
- Binnemans, K.; *Coord. Chem. Rev.* **2015**, *295*, 1.
- Rocha, L. A.; Avila, L. R.; Caetano, B. L.; Molina, E. F.; Sacco, H. C.; Ciuffi, K. J.; Calefi, P. S.; Nassar, E. J.; *Mater. Res.* **2005**, *8*, 361.
- Blasse, G.; *Chem. Phys. Lett.* **1975**, *33*, 616.
- Antic-Fidancev, E.; Hölsä, J.; Lastusaari, M.; *J. Alloys Compd.* **2002**, *341*, 82.
- Porcher, P.; Svoronos, D. R.; Leskelä, M.; Hölsä, J.; *J. Solid State Chem.* **1983**, *46*, 101.
- Antic-Fidancev, E.; *J. Alloy Compd.* **2000**, *300-301*, 2.
- Jüstel, T.; Möller, S.; Winkler, H.; Adam, W.; *Ullmann's Encyclopedia of Industrial Chemistry*, Wiley-VCH Verlag GmbH: Weinheim, 2012. DOI [10.1002/14356007.a15\\_519.pub2](https://doi.org/10.1002/14356007.a15_519.pub2).
- Rocha, L. A.; Ciuffi, K. J.; Sacco, H. C.; Nassar, E. J.; *Mater. Chem. Phys.* **2004**, *85*, 245.
- Yan, B.; Li, Q. P.; *Microporous Mesoporous Mater.* **2014**, *196*, 284.
- Shao, Y.-F.; Yan, B.; *Microporous Mesoporous Mater.* **2014**, *193*, 85.
- Gibelli, E.; Kai, J.; Teotonio, E.; Felinto, M.; Brito, H.; *J. Photochem. Photobiol., A* **2013**, *251*, 154.
- Werts, M. H. V.; Jukes, R. T. F.; Verhoeven, J. W.; *Phys. Chem. Chem. Phys.* **2002**, *4*, 1542.
- Basu, B. B. J.; Vasantharajan, N.; *J. Lumin.* **2008**, *128*, 1701.

51. Reisfeld, R.; Jørgensen, C. K. In *Handbook on the Physics and Chemistry of Rare Earths*; Gschneidner, K. A., Eyring, L., eds.; North Holland: Amsterdam, 1984.
52. Barve, R. A.; Suriyamurthy, N.; Panigrahi, B. S.; Venkatraman, B.; *Phys. B (Amsterdam, Neth.)* **2015**, 475, 156.
53. Santos, J. G.; Dutra, J. D. L.; Alves, S.; de Sá, G. F.; da Costa, N. B.; Freire, R. O.; *J. Braz. Chem. Soc.* **2013**, 24, 236.
54. Santa-Cruz, P. A.; Teles, F. S.; *Spectra Lux Software*; Ponto Quântico Nanodispositivos: Recife, 2003.
55. Fu, Z.; Geng, Y.; Chen, H.; Zhou, S.; Yang, H. K.; Jeong, J. H.; *Opt. Mater. (Amsterdam, Neth.)* **2008**, 31, 58.
56. Thirumalai, J.; Jagannathan, R.; Trivedi, D. C.; *J. Lumin.* **2007**, 126, 353.

Submitted: June 9, 2015

Published online: September 18, 2015

**FAPESP has sponsored the publication of this article.**